High-Speed Beam Steering With Phased Vertical Cavity Laser Arrays

Matthew T. Johnson, Dominic F. Siriani, Meng Peun Tan, and Kent D. Choquette, *Fellow, IEEE*

(Invited Paper)

***Abstract*—We demonstrate electronic beam steering using phased vertical cavity laser arrays at record high speed ($1.4{\cdot}10^8$ deg/s) and sensitivity to current (1.2 deg/100 μA). The relative phase and coherence between the array elements are extracted with a Fraunhoffer propagation method. The spatially resolved spectrum and beam steering dynamics are also analyzed. The thermo-optic effect is found to dominate the phase-shifting mechanism at lower speed steering, while the electronic variation in index dominates at higher speeds ($\geq$10 MHz).**

***Index Terms*—Beam steering, phased arrays, semiconductor laser arrays, semiconductor lasers.**

I. Introduction

OPTICAL phased array technology has been sought for several decades due to its promise of greater speed, accuracy, efficiency, and reliability than standard mechanical beam steering methods [1], [2]. The applications for this technology include fiber switching, free-space communications, and laser radar, and are as numerous and diverse as the approaches used, which can be generally classified into continuous and discrete methods. While optical phased arrays using liquid crystals are the most prominent for continuous steering [2], [3], alternative approaches include microelectromechanical systems [4], [5] electrowetting [6], surface gratings [7], waveguides [8]–[10], edge emitters [11], and vertical-cavity surface-emitting lasers (VCSELs) [12], [13].

Among the multiple figures of merit for optical beam steering, speed is still a limiting factor for applications such as laser radar. While mechanical methods clearly have inertial limitations, even the fastest methods using liquid crystals are limited to speeds under 10 kHz [14], [15]. Beam steering above the kilohertz regime has only been shown previously with grating and waveguide techniques, because rather than relying on mechanical or thermal changes, the index change with these methods can rely more directly on an electric field [8], [10] or current [16], [17]. These methods, however, are often difficult to extend into two dimensions, require elaborate setups with feedback control [8], are not conducive to free-space propagation [10], [16], or suffer from low efficiency [7].

A distinctive characteristic of the phased VCSEL array is that it acts as both the source and the beam steering mechanism. In this sense, it is a closer analog to its phased array radar counterpart. While all other methods alter the wavefront of an incident beam, with VCSEL arrays, we can adjust the phase of pixelated elements at their source. The primary advantages of this approach include a very high electro-optical efficiency, a natural extension into two dimensions [13], and fabrication with standard lithographic processes onto a small section of a semiconductor wafer.

As VCSEL arrays offer a fundamentally different approach, our understanding of the physical beam steering mechanism within them remains incomplete. The objective of this study is to further understand the steering mechanism, which will aid in optimizing these devices for particular applications.

We first describe the coherent VCSEL arrays in Section II, and discuss our method to extract the relative phase and coherence of the array elements in Section III. In Section IV, we compare the spatially resolved spectrum of the array elements under varying current injections to examine the beam steering mechanism. Section V reports a dynamic analysis of the arrays in the 100 Hz, 100 kHz, and 100 MHz regimes. We conclude in Section VI and show our data are consistent with carrier-induced thermal and electronic index mechanisms.

II. Phased VCSEL Array

A cross-sectional sketch of a 2×1 VCSEL array with a scanning electron microscope image inset is shown in Fig. 1. The VCSEL wafer used for the arrays consists of a p-type top distributed Bragg reflector (DBR) mirror with 27 periods and an n-type bottom DBR mirror with 35 periods on an n-type GaAs substrate. The active region located between the mirrors consists of three GaAs quantum wells that emit nominally at 850 nm. The photonic crystal hole pattern is designed to optically confine the mode within the defects, which are aligned with ion-implanted gain apertures of same size, the latter of which confine current to the individual elements. The fabrication procedure has been described in previous work [18], [19]. In an additional step, the top metal contact is etched with a focused ion beam to create electrical isolation between the contacts and allow preferential current injection into either element.

Manuscript received November 1, 2012; revised January 19, 2013; accepted January 20, 2013.

M. T. Johnson, M. P. Tan, and K. D. Choquette are with the Department of Electrical and Computer Engineering, University of Illinois at Urbana-Champaign, Urbana, IL 61801 USA (e-mail: mtjohns2@illinois.edu; mengtan@illinois.edu; choquett@illinois.edu).

D. F. Siriani is with the MIT Lincoln Laboratory, Lexington, MA 02420 USA (e-mail: dsiriani@gmail.com).

Color versions of one or more of the figures in this paper are available online at http://ieeexplore.ieee.org.

Digital Object Identifier 10.1109/JSTQE.2013.2244574

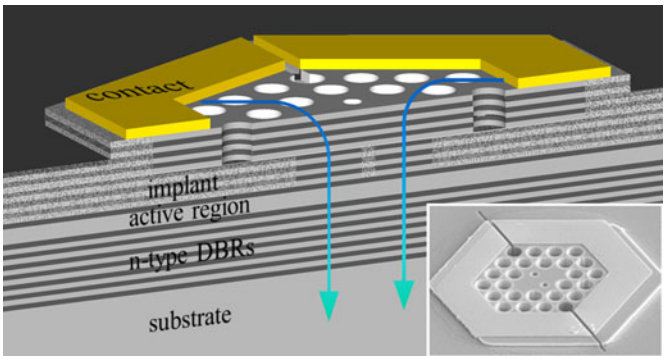

Fig. 1. 3-D sketch and scanning electron microscope image (inset) of a 2 × 1 VCSEL array.

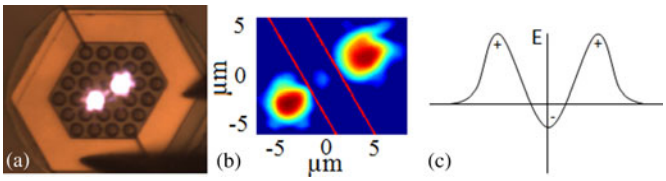

Fig. 2. (a) Near field and (b) processed image of a VCSEL array while lasing in the [+ − +] supermode. (c) Sketch of the electric field profile, where the smaller intensity central lobe is π out of phase with the outer lobes.

III. Phase and Coherence

A. Method

We first extract the relative phase and coherence between the array elements [20]. The near-field image in Fig. 2 shows the array operating in the "in-phase" supermode, with current separately applied to each element [20]. We designate this as the [+ − +] supermode since the electric field profile, as depicted in Fig. 2(c), has two zero crossings separating the three peaks [21]. After subtracting the background, the image is split into three different sections of the supermode, as delineated by the red lines shown in Fig. 2(b) [20].

The 2-D electric field amplitudes for each aperture are then obtained as the square root of the measured intensity, and are defined as $|U_{\text{left}}(\xi,\eta)|$, $|U_{\text{mid}}(\xi,\eta)|$, and $|U_{\text{right}}(\xi,\eta)|$, where ξ and η are the near-field coordinates. Approximating the fields in each of these apertures as self-coherent and monochromatic with flat wavefronts, the beam is then "propagated" to the far field using the Fraunhofer approximation [22]

$$U(x,y) = \frac{e^{jk_0 z}}{j\lambda_0 z} e^{j\frac{k_0}{2z}(x^2+y^2)} \iint_{-\infty}^{\infty} |U(\xi,\eta)|\, e^{j\frac{2\pi}{\lambda_0 z}(x\xi+y\eta)} d\xi d\eta \tag{1}$$

where x and y are the far-field coordinates, z is the propagation distance, and k_0 and λ correspond to the free-space wavelength. This approximation conveniently lends itself to a 2-D Fourier transform. The relative phase of the right aperture Φ_{right} and the magnitude of coherence between apertures $|\gamma|$ can then be fit according to

$$\begin{aligned} I(x,y) &= |U_{\text{left}}(x,y)|^2 + |U_{\text{mid}}(x,y)|^2 + |U_{\text{right}}(x,y)|^2 \\ &+ 2|\gamma|\text{Re}\left[\begin{array}{l} U_{\text{left}}(x,y)^* U_{\text{right}}(x,y) e^{j\Phi_{\text{right}}} \\ \quad + U_{\text{left}}(x,y)^* U_{\text{mid}}(x,y) e^{j\Phi_{\text{mid}}} \\ \quad + U_{\text{mid}}(x,y) e^{-j\Phi_{\text{mid}}} U_{\text{right}}(x,y) e^{j\Phi_{\text{right}}} \end{array}\right] \end{aligned} \tag{2}$$

where the propagated far-field intensity is denoted as $I(x,y)$, the relative phase of the middle aperture as Φ_{mid}, and the far fields propagated from the left, middle, and right apertures as $U_{\text{left}}(x,y)$, $U_{\text{mid}}(x,y)$, and $U_{\text{right}}(x,y)$, respectively. Since adjacent near-field lobes in phased VCSEL arrays typically have a π phase difference [23], [24], as per the sketch in Fig. 2(c), Φ_{mid} is assumed to be π out of phase with the average phase of the two outer apertures.

The parameters Φ_{right} and γ can then be extracted by matching the far-field measurements obtained with a goniometric radiometer to the far field propagated from the near field using (1) and (2). The relative phase is first determined in an iterative process until the relative amplitudes of the left and right far-field lobes match those determined experimentally. This method is used in contrast to that of previous works where the angular shifts are matched [19], [25], because it is less subject to experimental error. Similarly, the coherence between elements is determined by matching the relative amplitude of the far-field nulls.

Near- and far-field measurements are taken over the range of coherent operation of each array for fixed current injection through the left contact, and varying current injection into the right contact. The experimental and propagated-fit far-field profiles are compared in Fig. 3, where the 2-D profiles shown above the plot depict the slices where the 1-D profiles are taken [20]. It is noteworthy that the near-field central lobe contained in $|U_{\text{mid}}(\xi,\eta)|$, in spite of its low intensity, has significant influence on the relative intensity of the far-field lobes. For this reason, the experimentally determined near field, as opposed to the typical Gaussian approximations used, leads us to a more accurate far-field simulation, and therefore more accurate phase retrieval.

B. Phase

It can be seen in Fig. 3 that as the current to the right element is increased, the far field is pulled to the right over a beam steering range of 2°. This is caused by a linearly increasing relative phase lag in the right element, as plotted in Fig. 4 [20]. The maximum beam steering range is determined by the spacing between elements, which also determines the dominant supermode [18]. Note also from this figure that the observed phase range of coherent operation extends about 0.5π in either direction of the preferred phase relation between the elements (in-phase). Beyond this phase range, the array approaches the [+ −], or "out-of-phase," supermode, which leads to a dramatic decrease in coherence [26].

While ≈20 mA current difference has been reported to obtain a π phase shift in slab-coupled lasers [27], we demonstrate

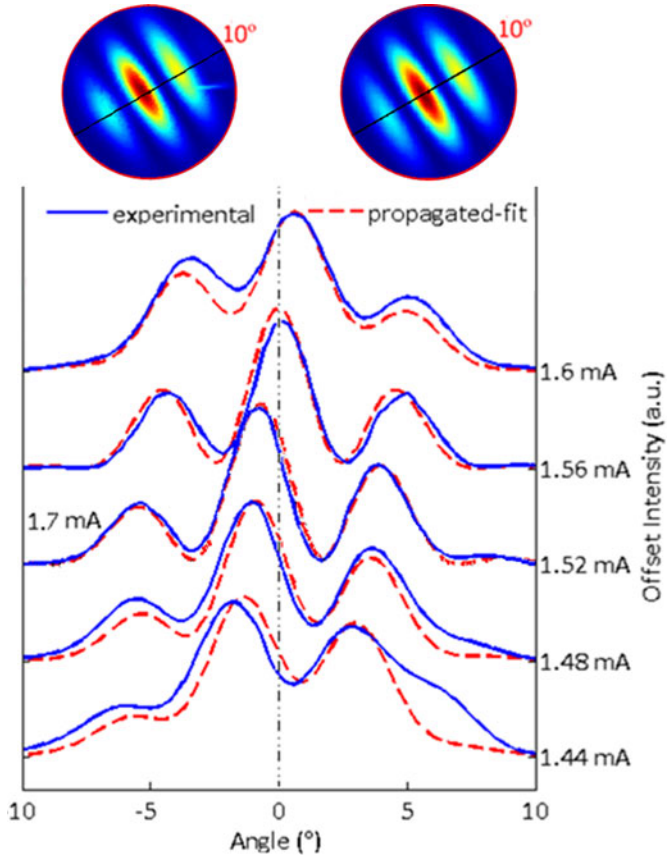

Fig. 3. Typical 2-D profiles of the measured and propagated-fit far fields and 1-D far-field profiles under fixed (varying) current to the left (right) contact.

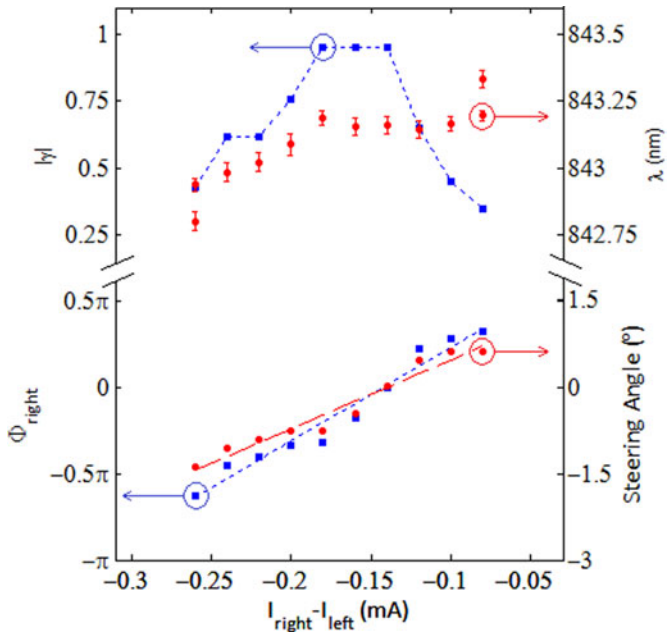

Fig. 4. Relative phase, coherence, wavelength, and steering angle versus current difference between left and right elements.

this same phase shift over a differential current spread of only 170 μA. The fit lines in Fig. 4 correspond to record-high phase and steering rates of 0.54π and 1.2° per 100 μA, respectively.

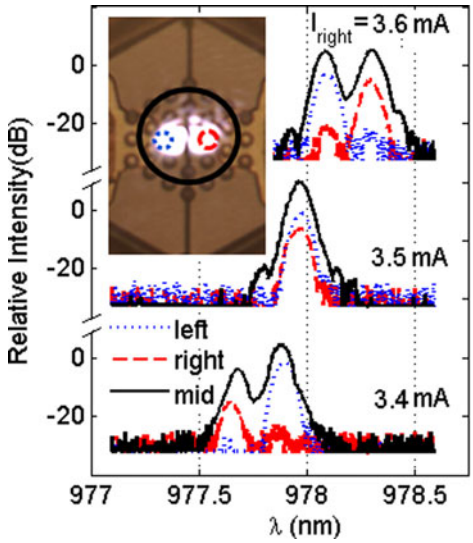

Fig. 5. Spatially resolved spectra obtained from a magnified image onto 9 μm (left and right) and 65 μm (middle) diameter core fiber. Current to the left element was held at 3.6 mA, while current to the right element was varied. Inset shows the approximate locations and diameters contributing to the spectra shown.

This sensitivity relies on strong current confinement between the array elements, which is dependent in our arrays on both the ion implantation and the depth of the channel cut between the contacts with a focused ion beam.

C. Coherence

The coherence magnitude and emission wavelength are also plotted against the current difference in Fig. 4 [20]. While the array elements are highly coherent around their preferred operation with no phase difference, they lose coherence as they are pulled away from it. This loss of coherence is also associated with the onset of a competing mode, as shown by the dual emission peaks found at either end of the current difference in Fig. 4. This corroborates previous results showing a reduction in coherence when operated away from the preferred in-phase or out-of-phase condition [26], and upon the onset of another spectral mode [28].

IV. Array Spectrum

In order to elucidate the beam steering mechanism and to characterize the array modes, we examine the spatially resolved spectrum of each element in a VCSEL array operating near 980 nm. This array operates in conditions similar to that of the 850-nm array shown in Figs. 3 and 4, where spectral splitting is observed with increased current difference and identical beam steering behavior is observed. Hence, these results are independent of the emission wavelength.

Fibers with 9- and 62.5-μm diameter cores are placed at a magnified image plane of the near field to capture the spatially resolved spectra. The 65-μm core fiber was used to capture the spectra encompassing both elements, while the 9-μm core fiber was used to capture the spectra of the left and right elements. The inset in Fig. 5 shows the approximate positions of the fiber

in the near field where the spectra were obtained from. Fig. 5 also shows the spectra obtained with fixed current to the left element (3.6 mA) and varying current to the right element at the different locations/diameters shown by the inset. The array operates coherently with 3.5 mA to the right element, but is pulled out of coherence and into two spectral modes at 3.4 and 3.6 mA (similar to the largest and smallest current difference in Fig. 4). Between these extremes, there is a current range of 0.12 mA with high coherence and SMSR >30 dB. In this current range in Fig. 5, we see similar coherent behavior as that shown in Fig. 4.

It is observed that at higher current to the right element, while the overall spectra are red-shifted, the right element is lasing at a predominantly longer wavelength than the left element. Similarly, with lower current to the right element, the spectra are blue-shifted, while the right element is lasing at a predominantly shorter wavelength than the left element. The spectral data thus reveal that as the current to a given element is increased with respect to the other, its respective resonant wavelength also increases. This is consistent with the thermo-optic effect for GaAs and AlAs, where $\partial n/\partial T \approx 4{\cdot}10^{-4}$ and $1{\cdot}10^{-4}$ K^{-1}, respectively [29], [30].

The coherence and spectral data from Figs. 4 and 5 thus suggest that as the resonant wavelength difference between the elements increases with increasing current difference, the elements are eventually decoupled and the coherence is lost. The phase extraction of Fig. 3 informs us that when current injection to an element is increased under continuous wave operation, the part of the supermode emanating from that element incurs a relative phase lag.

V. Beam Steering Dynamics

A. 100 Hz

We first characterize beam steering at low modulation speeds with an array similar to that shown in Fig. 2, which emits at 850 nm. The current to the left array element is held constant, while the current to the right element is modulated in a square wave with a pattern generator between 3.06 and 3.13 mA at 100 Hz. A photoreceiver located 6 cm from the VCSEL array and subtending a 0.8° angular width is then translated across the far field as indicated in Fig. 6 [31].

A temporal plot of injected current is also shown in Fig. 6 along with the detected signal at the angular locations of 0° and 3°. With the detector placed at 0°, the optical signal is found to rise and fall with the current to the right element. At 3°, however, the detected signal varies oppositely with the injected signal. At each of these measurement angles, the photocurrent value is averaged over the times of the low and high input signals, which gives us two points in the far field. The detector is then translated to detect these values at angular increments, and the far-field profiles corresponding to the low and high current values, shown in Fig. 6, are obtained.

The dynamic far-field data show that at higher currents, the far-field profile is shifted to the right over a range of ≈0.8°, which is consistent with the dc measurements obtained from the goniometric radiometer, shown by the dotted lines in Fig. 6. Using the phase extraction technique described in Section III [20], we find that a current change of only 70 μA into the right element gives a phase shift of 0.3π, corresponding to approximate phase and steering rates of 0.4π and 1.1° per 100 μA, respectively.

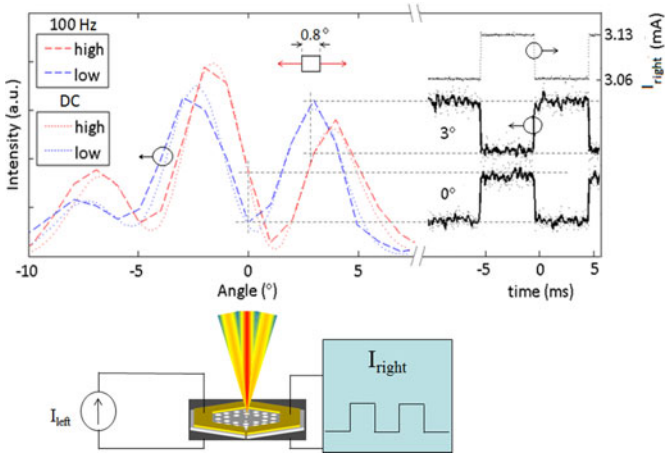

Fig. 6. (a) Far-field profiles obtained from translating photoreceiver at 100 Hz (dashed) and from goniometric radiometer with dc current (dotted). The far-field data points at high and low currents to the right element are obtained from the time-domain photocurrent signals, shown at angular locations of 0° and 3°.

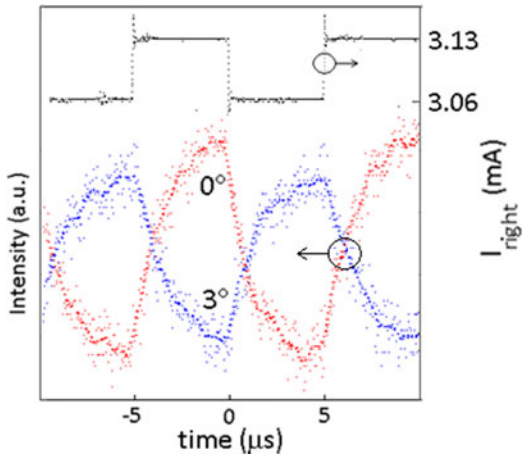

Fig. 7. Photocurrent obtained at the angular positions of 0° and 3°, while the right element current is modulated at 100 kHz.

B. 100 kHz

Next, the modulation rate is increased to 100 kHz. At this speed, we find that the far-field profile continues to shift to the right with higher current to the right element, consistent with measurements at 100 Hz and dc. However, as seen by the temporal dependence of the spatially resolved signals in Fig. 7, a rise/fall time on the order of 5 μs is evident [31]. Similar delays between 1 and 20 μs for steering and the onset of lasing are observed in GaAs VCSELs dependent on thermal lensing [32]–[34]. The observed rise/fall time in Fig. 7 is therefore consistent with a thermally dominated beam steering mechanism. The increase of current to the right element is accompanied by an increase to the relative temperature on that side of the array, which increases the relative index on that side

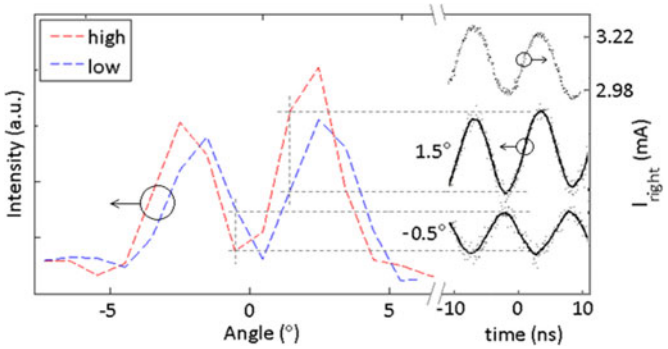

Fig. 8. Far-field profiles at 100 MHz obtained from translating photoreceiver. Profiles extracted from time-domain photocurrent at the angular locations of -0.5 and 1.5°.

in accordance with the thermo-optic effect. The beam steering arising from the thermo-optic effect is thus limited to the kilohertz regime.

C. 100 MHz

However, if we increase the modulation rate beyond the temporal limits of the temperature response, we see an entirely different beam steering phenomena. Using the same setup as that in Fig. 6, but with a modulation speed of 100 MHz, we obtain the far-field profiles shown in Fig. 8 [31]. The steering shown corresponds to a record high angular speed of $1.4{\cdot}10^8$ °/s over a beam steering range of $\approx 0.7^\circ$. The difference at this modulation rate, however, is that we find the beam is steered to the *left* with increased current to the right element. The relative phase lag in the right element is estimated as -0.2π for a current increase into the right element of 240 μA [20], which corresponds to approximate phase and steering rates of -0.08π and -0.4° per 100 μA. The reduced phase and steering rates in the opposite direction are consistent with an electronic index change, where the index is suppressed with increasing current as $\partial n/\partial N \approx -10^{-21}$ cm^3 [35].

VI. Conclusion

While the thermo-optic effect is found to dominate at dc and slower modulation rates, when we modulate at faster rates ($\geq$10 MHz), the thermal dynamics are effectively neutralized since the temperature cannot respond as quickly as the current. The weaker and opposite effect of the electronic index change, where the index decreases with increasing current, is then found as the dominant phase-shifting mechanism.

We have extracted the relative phase and coherence of phased vertical cavity laser arrays with a unique method using the experimentally determined near and far fields. We have also examined the spatially resolved spectra and the beam steering dynamics, both of which are consistent with the thermo-optic effect dominating the phase-shifting mechanism at lower speeds. Dynamic testing at speeds greater than 10 MHz revealed that the electronic index change dominates in this regime. A record, equipment-limited steering speed and sensitivity to current for free-space beam steering have also been demonstrated with our phased VCSEL array. Simulations have shown such arrays to be capable of switching speeds over 40 GHz, well above the typical modulation limit of VCSELs imposed by the relaxation oscillation frequency [36]. Future effort will be needed to increase the steering angle range, decrease the central lobe divergence, and to further elucidate the phase-shifting mechanism.

References

[1] P. F. McManamon, T. A. Dorschner, D. L. Corkum, L. J. Friedman, D. S. Hobbs, M. Holz, S. Liberman, H. Q. Nguyen, D. P. Resler, and R. C. Sharp, "Optical phased array technology," *Proc. IEEE*, vol. 84, no. 2, pp. 268–298, Feb. 1996.

[2] P. F. McManamon, P. J. Bos, M. J. Escuti, J. Heikenfeld, S. Serati, H. Xie, and E. A. Watson, "A review of phased array steering for narrow-band electrooptical systems," *Proc. IEEE*, vol. 97, no. 6, pp. 1078–1096, Jun. 2009.

[3] S. R. Davis, G. Farca, S. D. Rommel, S. Johnson, and M. H. Anderson, "Liquid crystal waveguides: New devices enabled by$>$ 1000 waves of optical phase control," *Emerging Liq. Cryst. Technol. V*, vol. 7618, pp. 76180E-1–76180E-14, 2010.

[4] A. Tuantranont, V. Bright, J. Zhang, W. Zhang, J. Neff, and Y. Lee, "Optical beam steering using MEMS-controllable microlens array," *Sens. Actuators A, Phys.*, vol. 91, pp. 363–372, 2001.

[5] U. Krishnamoorthy, K. Li, K. Yu, D. Lee, J. Heritage, and O. Solgaard, "Dual-mode micromirrors for optical phased array applications," *Sens. Actuators A, Phys.*, vol. 97, pp. 21–26, 2002.

[6] N. R. Smith, D. C. Abeysinghe, J. W. Haus, and J. Heikenfeld, "Agile wide-angle beam steering with electrowetting microprisms," *Opt. Exp.*, vol. 14, pp. 6557–6563, 2006.

[7] J. K. Doylend, M. Heck, J. T. Bovington, J. D. Peters, L. Coldren, and J. Bowers, "Two-dimensional free-space beam steering with an optical phased array on silicon-on-insulator," *Opt. Exp.*, vol. 19, pp. 21595–21604, 2011.

[8] W. R. Huang, J. Montoya, J. E. Kansky, S. M. Redmond, G. W. Turner, and A. Sanchez-Rubio, "High speed, high power one-dimensional beam steering from a 6-element optical phased array," *Opt. Exp.*, vol. 20, pp. 17311–17318, 2012.

[9] X. Gu, T. Shimada, A. Fuchida, A. Matsutani, A. Imamura, and F. Koyama, "Ultra-compact beam-steering device based on Bragg reflector waveguide amplifier with number of resolution points over 100," *Electron. Lett.*, vol. 48, no. 6, pp. 336–337, Mar. 2012.

[10] M. Jarrahi, R. F. W. Pease, D. A. B. Miller, and T. H. Lee, "Optical switching based on high-speed phased array optical beam steering," *Appl. Phys. Lett.*, vol. 92, pp. 014106-1–014106-3, 2008.

[11] E. Kapon, Z. Rav-Noy, L. Lu, M. Yi, S. Margalit, and A. Yariv, "Phase-locking characteristics of coupled ridge waveguide InP/InGaAsP diode lasers," *Appl. Phys. Lett.*, vol. 45, pp. 1159–1161, 1984.

[12] T. Ide, M. Shimizu, S. Mukai, M. Ogura, T. Kikuchi, Y. Suzuki, R. Kaji, H. Itoh, M. Watanabe, and H. Yajima, "Continuous output beam steering in vertical-cavity surface-emitting lasers with two p-type electrodes by controlling injection current profile," *Jpn. J. Appl. Phys.*, vol. 38, pp. 1966–1970, 1999.

[13] D. F. Siriani and K. D. Choquette, "Electronically controlled two-dimensional steering of in-phase coherently coupled vertical-cavity laser arrays," *IEEE Photon. Technol. Lett.*, vol. 23, no. 3, pp. 167–169, Feb. 2011.

[14] G. D. Love, A. K. Kirby, and R. A. Ramsey, "Sub-millisecond, high stroke phase modulation using polymer network liquid crystals," *Opt. Exp.*, vol. 18, pp. 7384–7389, 2010.

[15] J. Sun, R. A. Ramsey, Y. Chen, and S. T. Wu, "Submillisecond-response sheared polymer network liquid crystals for display applications," *J. Disp. Technol.*, vol. 8, pp. 87–90, 2012.

[16] X. Dong, P. LiKamWa, J. Loehr, and R. Kaspi, "Current-induced guiding and beam steering in active semiconductor planar waveguide," *IEEE Photon. Technol. Lett.*, vol. 11, no. 7, pp. 809–811, Jul. 1999.

[17] W. Guo, P. Binetti, C. Althouse, H. Ambrosius, L. Johansson, and L. A. Coldren, "Very fast ($>10^7$ degree/s) 2D optical beam steering through an InP phtotonic integrated circuit," in *Proc. IEEE Photon. Conf.*, Burlingame, CA, USA, Sep. 2012, pp. 842–843.

[18] D. F. Siriani and K. D. Choquette, "Implant defined anti-guided vertical-cavity surface-emitting laser arrays," *IEEE J. Quantum Electron.*, vol. 47, no. 2, pp. 160–164, Feb. 2011.

[19] A. C. Lehman, J. J. Raftery, Jr., A. J. Danner, P. O. Leisher, and K. D. Choquette, "Relative phase tuning of coupled defects in photonic

crystal vertical-cavity surface-emitting lasers," *Appl. Phys. Lett.*, vol. 88, pp. 021102–021103, 2006.
[20] M. T. Johnson, D. F. Siriani, J. D. Sulkin, and K. D. Choquette, "Phase and coherence extraction from a phased vertical cavity laser array," *Appl. Phys. Lett.*, vol. 101, pp. 031116–031119, 2012.
[21] E. Kapon, J. Katz, and A. Yariv, "Supermode analysis of phase-locked arrays of semiconductor lasers," *Opt. Lett.*, vol. 9, pp. 125–127, 1984.
[22] J. W. Goodman, *Introduction to Fourier Optics*. Englewoods, CO, USA: Roberts & Company Publishers, 2005.
[23] D. K. Serkland, K. Choquette, G. Hadley, K. Geib, and A. Allerman, "Two-element phased array of antiguided vertical-cavity lasers," *Appl. Phys. Lett.*, vol. 75, pp. 3754–3756, 1999.
[24] L. D. A. Lundeberg and E. Kapon, "Mode switching and beam steering in photonic crystal heterostructures implemented with vertical-cavity surface-emitting lasers," *Appl. Phys. Lett.*, vol. 90, pp. 241115–241117, 2007.
[25] L. D. A. Lundeberg, G. P. Lousberg, D. L. Boiko, and E. Kapon, "Spatial coherence measurements in arrays of coupled vertical cavity surface emitting lasers," *Appl. Phys. Lett.*, vol. 90, pp. 021103–021105, 2007.
[26] A. C. Lehman, J. J. Raftery, P. S. Carney, and K. D. Choquette, "Coherence of photonic crystal vertical-cavity surface-emitting laser arrays," *IEEE J. Quantum Electron.*, vol. 43, no. 1, pp. 25–30, Jan. 2007.
[27] R. K. Huang, B. Chann, L. J. Missaggia, S. J. Augst, R. B. Swint, J. P. Donnelly, A. Sanchez-Rubio, and G. W. Turner, "High-power coherent beam combination of semiconductor laser arrays," presented at the Conf. Lasers Electro-Optics, San Jose, CA, USA, 2008.
[28] D. F. Siriani, P. S. Carney, and K. D. Choquette, "Coherence of leaky-mode vertical-cavity surface-emitting laser arrays," *IEEE J. Quantum Electron.*, vol. 47, no. 5, pp. 672–675, May 2011.
[29] D. Marple, "Refractive index of GaAs," *J. Appl. Phys.*, vol. 35, pp. 1241–1242, 1964.
[30] H. Grimmeiss and B. Monemar, "Temperature dependence of the refractive index of AIAs and AIP," *Phys. Status Solidi (a)*, vol. 5, pp. 109–114, 1971.
[31] M. T. Johnson, D. F. Siriani, and K. D. Choquette, "Beam steering modulation with phased vertical cavity laser arrays," in *Proc. IEEE Photon. Conf.*, Burlingame, CA, USA, Sep. 2012, pp. 242–243.
[32] N. K. Dutta, L. W. Tu, G. Hasnain, G. Zydzik, Y. H. Wang, and A. Y. Cho, "Anomalous temporal response of gain guided surface emitting lasers," *Electron. Lett.*, vol. 27, no. 3, pp. 208–210, Jan. 1991.
[33] G. Hasnain, K. Tai, L. Yang, Y. Wang, R. Fischer, J. D. Wynn, B. Weir, N. Dutta, and A. Cho, "Performance of gain-guided surface emitting lasers with semiconductor distributed Bragg reflectors," *IEEE J. Quantum Electron.*, vol. 27, no. 6, pp. 1377–1385, Jun. 1991.
[34] M. I. Cohen, A. A. Allerman, K. D. Choquette, and C. Jagadish, "Electrically steerable lasers using wide-aperture VCSELs," *IEEE Photon. Technol. Lett.*, vol. 13, no. 6, pp. 544–546, Jun. 2001.
[35] B. R. Bennett, R. A. Soref, and J. A. Del Alamo, "Carrier-induced change in refractive index of InP, GaAs and InGaAsP," *IEEE J. Quantum Electron.*, vol. 26, no. 1, pp. 113–122, Jan. 1990.
[36] P. M. Goorjian and C. Z. Ning, "Ultrafast beam self-switching by using coupled vertical-cavity surface-emitting lasers," *J. Modern Opt.*, vol. 49, pp. 707–718, 2002.

Matthew T. Johnson received the B.S. degree in electrical and electronics engineering from Oregon State University, Corvallis, OR, USA, in 2002, and the M.S. degree in electro-optics from the Air Force Institute of Technology (AFIT), Wright Ptrsn AFB, OH, USA, in 2007.

He was the Program Manager of the C4ISR Enterprise Integration System Program, Hanscom Air Force Base. Upon graduating from the AFIT, he joined the Munitions Directorate, Air Force Research Laboratory, where he became a Team Leader for infrared scene projection, the Section Chief of the Advanced Fuzes Section, and the Branch Chief of the Weapons Dynamics and Controls Sciences Branch. He is currently with the Department of Electrical and Computer Engineering, University of Illinois at Urbana-Champaign, Urbana, IL, USA. His research interests include vertical-cavity surface-emitting lasers, optical phased arrays, and electro-optical characterization.

Mr. Johnson is a Student Member of the IEEE Photonics Society.

Dominic F. Siriani received the B.S., M.S., and Ph.D. degrees in electrical engineering from the University of Illinois at Urbana-Champaign, Urbana, IL, USA, in 2006, 2007, and 2011, respectively.

In 2011, he joined MIT Lincoln Laboratory, Lexington, MA, USA, where he is currently a technical staff member of the Electro-Optical Materials and Devices Group. His research interests include vertical-cavity surface-emitting lasers, diode laser arrays, diode laser design and characterization, and coherence theory.

Dr. Siriani is a member of the IEEE/Photonics Society and the Optical Society of America.

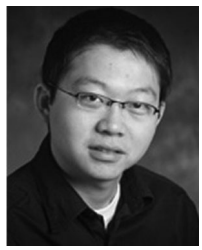

Meng Peun Tan received the B.S., M.S., and Ph.D. degrees in electrical engineering from the University of Illinois at Urbana-Champaign, Urbana, IL, USA, in 2007, 2009, and 2013, respectively.

He is currently with the Department of Electrical and Computer Engineering, University of Illinois at Urbana-Champaign. His current research interests include mode control in semiconductor lasers, various high-speed laser modulation schemes in vertical-cavity surface-emitting lasers, as well as active and passive devices in optical interconnects.

Dr. Tan is a member of the IEEE photonics Society.

Kent D. Choquette (M'97–F'03) received the B.S. degrees in engineering physics and applied mathematics from the University of Colorado-Boulder, Boulder, CO, USA, and the M.S. and Ph.D. degrees in materials science from the University of Wisconsin-Madison, Madison, WI, USA.

He was a Postdoctoral Researcher at AT&T Bell Laboratories, Murray Hill, NJ. He then joined Sandia National Laboratories, Albuquerque, NM. In 2000, he joined the Department of Electrical and Computer Engineering, University of Illinois at Urbana-Champaign, where he was named the Able Bliss Professor of Engineering. His research in Photonic Device Research Group is centered around the design, fabrication, characterization, and applications of vertical-cavity surface-emitting lasers, photonic crystal light sources, nanofabrication technologies, and hybrid integration techniques. He has authored more than 200 technical publications and five book chapters, and has presented numerous invited talks and tutorials.

Dr. Choquette was an Associate Editor of the IEEE JOURNAL OF QUANTUM ELECTRONICS, the IEEE PHOTONIC TECHNOLOGY LETTERS, and the JOURNAL OF LIGHTWAVE TECHNOLOGY, as well as a Guest Editor of the IEEE JOURNAL OF SELECTED TOPICS IN QUANTUM ELECTRONICS. He received the 2012 Optical Society of America (OSA) Nick Holonyak Jr. Award and the 2008 IEEE/Lasers and Electro-Optics Society (LEOS) Engineering Achievement Award. From 2000 to 2002, he was an IEEE/LEOS Distinguished Lecturer. He is a Fellow of the OSA, a Fellow of the International Society for Optical Engineers, and a Fellow of the American Association for the Advancement of Science.